In: IEEE/AIAA 42nd Digital Avionics Systems Conference (DASC) 2023, 1-5 October 2023, Barcelona, Spain
DOI:10.1109/DASC58513.2023.10311317

# Dynamic separation minima prediction with collision risk modelling (CRM)

Christantus O. Nnamani, Tingyu Gong, Yan Xu, Antonios Tsourdos
*School of Aerospace, Transport and Manufacturing*
*Cranfield University*
Bedford, United Kingdom
{christantus.nnamani, tingyu.gong, yanxu, a.tsourdos}@cranfield.ac.uk

***Abstract*— In this paper, we modelled the geometry between 2 proximate aircraft as an oblate-spheroid and obtained a collision risk model based on collision probability. The methodology entails translating the communication, navigation and surveillance error characteristics, and wind uncertainty into the spatial domain of spheroid. Furthermore, we used the collision probability to design a dynamic separation minima based on the parameters of the oblate-spheroid geometry. The results showed that by varying the parameters of the spheroid, allows for a dynamic setting of the separation minima. The collision probability was compared to Monte Carlo simulations as a baseline model. Therefore we proposed a dynamic configuration of the separation minima between aircraft as a function of the collaborative geometry to increase the airspace capacity, especially with great demand from unmanned operations.**

***Keywords*—Collision model, risk, manned and unmanned aircraft, separation minima, CRM, collision probability**

## I. Introduction

Future airspace will be a mixture of manned and unmanned aircraft with diverse functionalities and applications. These aircraft will safely share the limited aerial resources and thus needs to be managed appropriately to reduce conflict risks. The safe managerial integration of future aviation applications is the primary objective of this paper supporting research explorations of high-intensity autonomous drone operations (HADO) and BLUEPRINT projects. These integration techniques support many air aircraft sharing current aviation airspace and creating other operation dimensions like unmanned operations below 400ft [1]. Although safety is critical in the integration of diverse aircraft into the airspace, the increased utilisation of the airspace by different aircraft increases the probability or risk of collision. Therefore, to account for the variation in application integration and increase utilisation, a redesign of the collision risk modelling associated with airspace operation is necessary. We note that several collision risk models have been developed over the years for manned operations [2] and recently extended to unmanned operations [3]. Nevertheless, these models considered both operations as independent entities, thereby limiting the concept of integrated operations as required for future airspace. In this paper, we propose a collision risk model that considers the integrated airspace where manned and unmanned operations co-occur.

This work was supported in part by the UKRI Future Flight Challenge Phase 3 programmes under project Blueprint (ID: 10025964) and HADO (High-intensity Autonomous Drone Operations) (ID: 10024815).

Furthermore, for aerial aircraft collision to occur, two or more aircraft or their parts must overlap in the vertical, lateral, and longitudinal planes at an instantaneous time [4]. Hence, the geometry of the aircraft is fundamental as it describes part of the dynamics of the aircraft. We considered the dynamics of the aircraft in terms of position and velocity to propose the collision risk management model. The aircraft's velocities were presumed to be constant in magnitude and direction during the possible collision period. This is justified since a change in velocity leads to aircraft manoeuvring that impacts the conflict area. We model the aircraft, which can be manned or unmanned, as an ellipsoid with a radius of the longest axis spanning half of the cross-sectional length of the longest part of the aircraft in addition to uncertainty due to wind impact on the aircraft. The air aircraft geometrical model allowed for a generalisation of the aircraft type - manned or unmanned (small or large).

Following the definition of the aircraft model, we formulate and describe the collision position and velocity constraints. These constraints were used to define the collision probabilities with other collision conflict parameters and required target level of safety as variables. Therefore, the methodology deployed in the paper entails translating the communication, navigation and surveillance error characteristics, and wind uncertainty into the spatial domain of the ellipsoid defining the aircraft geometry thereby, forming a virtual risk protection disk around the aircraft. Since the main objective of the collision risk model developed as a function of the conflict probabilities is to optimise conflict resolution decision techniques. The decision techniques including response time and manoeuvrability are a trade-off between accuracy and efficiency. Therefore, the collision risk model proposed herein characterises the decision techniques by allowing for conflict probability assessment. The results obtained recommended the dynamic configuration of the separation minima between aircraft as a function of their geometry. This observation is critical as it increases the safe usability of the airspace for multiple operations especially when airspace volume restriction is not enforced.

## II. Related work

Conflict estimation for air traffic is essential for the safe operation of the aviation sector, however, it comprises several uncertainties due to the probabilistic nature of the responsible actors. Such actors range from human interaction, equipment functionalities and environmental impact. Due to these uncertainties, conflict estimation relies on theoretical probabilistic models such as evaluating the absorbing and transient boundary interactions using the Markov process discussed in [2]. However, all the probabilistic models rely on the accuracy of the relative information about the aircraft, such as its position, speed and onboard equipment. Errors arising from the measurements and transmission of the aircraft information have been studied in literature with modalities to improve the accuracy. We note that to account for these errors in establishing conflict management procedures, separation minima were incorporated with safety margins to allow for collision mitigation [5]. The safety margins are represented in response time or separation distance to allow for mitigation. Hence, the separation minima can be time-based or distance-based [6].

Positioning error was examined in [7] as limiting accurate separation and a dynamic formulation of the dimensions of the aircraft's position was proposed to compensate for the positioning error. In addition, the role of human interaction and errors relating to aircraft separation was evaluated with results postulating a time-based separation $> 50s$ to account for the human errors [8]. The primary cause of human error to maintain separation was based on control and decision response. Therefore, interactive software was developed for collision risk estimation considering the limits of separation minima defined by the International Civil Aviation Organization (ICAO) in [9]. The evaluation of these human errors is essential for prompt response to avoid collision and total loss of separation. However, since the establishment of conflicts is probabilistic, the separation minima can be mapped to a risk measure characterising possible errors. For standardization and accounting purposes, the separation minima are also linked to a target value of the ICAO's Target Level of Safety (TLS) [4], [6].

The safety analysis for operations below 800ft showed a $5\%$ required vertical separation distribution [10] which supports most unmanned aircraft operations. Although regulations on operation intent declaration and authorisation, geo-fencing, etc., prescribe separation for unmanned operations, it does not fully account for the separation of small unmanned aerial system (sUAS) interaction with manned operations. While separation minima standards have been statically defined for manned aviation by ICAO in [11, Chapter 3], the standards for unmanned aircraft have not been assembled by ICAO. This is because unmanned operations have introduced unique challenges in defining altitude referencing to other aviation operations [12]. However, for sUAS, the American Society for Testing and Materials (ASTM) adopted the hockey puck recommendation proposed in [13] with lateral by vertical dimension of 2000ft by 250ft as the well-clear boundary and 500ft by 100ft as the near-mid-air-collision (NMAC) boundary [14]. Large UAS typically have a lateral and vertical well-clear boundary of 4000ft by 450ft [13].

Furthermore, with growing applications of unmanned operations and advancements in communication, navigation and surveillance (CNS) equipment used by both manned and unmanned aircraft, the ICAO's separation standards are becoming sub-optimal. By evaluating the ICAO's separation standards on Singapore's procedural airspace, evidence showed that the advances in CNS equipment allow for a reduction of lateral and longitudinal separation standards from 50NM to 22NM and 20NM respectively while maintaining the TLS [9]. As the technologies continue to grow, it is apparent that the static definition of separation minima of different interacting aircraft would become less optimal and difficult to sustain as competition for aerial resources increases.

Hence, dynamic separation is required as a panacea to its static counterpart. Using Bayesian network prediction and safety performance functions, separation minima infringements were computed to ameliorate the characterisation of static separation and determine safe air routes [10]. We note that the concept of dynamic separation had been presented in the literature as a solution to specific airspace challenges. Dynamic separation was proposed as a mechanism to optimise safe separation due to the capacity limitation introduced by procedural static separation when wake vortexes occur [15]. In addition to human error and aircraft equipment, wake vortex is a factor considered when determining the separation minima as experiments showed that wake vortex trail retains enough energy to interfere with another aircraft up to 40 wingspans [4], [15].

## III. Conflict and separation model

In this section, we discuss the formulations for the dynamic separation minima and collision risk model. We present a description of the generalised aircraft geometry, the analytical derivations of the conflict probabilities and the deduction to the dynamic separation minima.

### A. Aircraft geometry

The aircraft geometry follows an ellipsoid geometry which literally encloses the aircraft within an ellipsoid shape like a sphere or cylinder, etc. [3]. The 3D presentation of a typical aircraft shows varying axis lengths in the 3D space, therefore leading to a tri-axial ellipsoid. The ellipsoidal geometry allows for a variety of aircraft such as the UA, GA and manned aircraft, etc. Other possible geometries of aircraft are depicted in fig.1.

The Reich collision model simplifies the geometry of an aircraft by assuming that aircraft shapes are represented in a 3D box [16]. By considering the boundary conditions at the collision interface, the Reich model can be extended to cover air traffic models along any network [2]. However, we present the ellipsoidal geometry of an aircraft encompassing required safety margins in this paper to generalise the collision model.

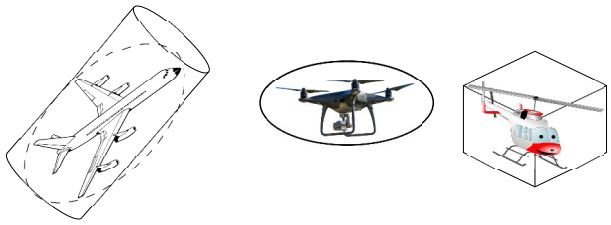

Fig. 1. The geometry of aircraft

When an aircraft is in motion, 2 types of errors - cross-track and along-track- are responsible for aircraft deviations. These errors are primarily caused by the effect of wind on the aircraft and are mitigated by advanced stability controls. The cross-track errors with a magnitude less than 0.5NM for aircraft with a flight management system (FMS) are maintained by a lateral feedback loop. In contrast, the along-track (more significant) errors require longitudinal controls like an automatic throttle to compensate for the errors. These errors typically affect the parts of the aircraft in the 3D space. Therefore, to model the dimension of the aircraft, an error margin is necessary for the 3D of the aircraft ellipsoid. By analysing data from 4000 flights, the along-track error (forward track prediction) follows closely a normal distribution [17]. Furthermore, evaluating the prediction of the aircraft, the prediction errors taking into consideration the cross-track and along-track errors represent an ellipse in 2D and extended to an ellipsoid in 3D space [17]. This assertion provides that for the computational procedure, the geometry of the aircraft in 3D space can be represented as an ellipsoid. However, the choice of the type of ellipsoid depends on the axis of the ellipsoid which relates to the physical dimensions of the aircraft.

Let us define an analytical ellipsoid with the centre of mass located at $C = \{c_0, c_1, c_2\}$ representing an aircraft as (1).

$$\left(\frac{x_0}{a_0}\right)^2 + \left(\frac{x_1}{a_1}\right)^2 + \left(\frac{x_2}{a_2}\right)^2 = 1, \tag{1}$$

where $a_i$ and $x_i$ represent the length of the aircraft axis and the coordinate of a point on the surface of the ellipsoid respectively. We note that $a_0 \geq a_1 \geq a_2 > 0$. If $a_0 = a_1 = a_2$ then the ellipsoid is a sphere, however, if $a_0 \neq a_1 \neq a_2$, $a_0 = a_1 > a_2$, $a_0 = a_1 < a_2$ the shape becomes a tri-axial ellipsoid, oblate spheroid, and prolate spheroid respectively. We note that the configuration of the aircraft shapes can lead to an oblate or prolate spheroid depending on the configuration of the 2 equal axes to the third axis. However, we assume in this paper that the ellipsoidal representation is an oblate spheroid.

### *B. Collision position*

Figure 2 presents the pictorial representation of the collision of 2 oblate-spheroid-based aircraft. The choice of the shapes of the aircraft ensures that the collision model is applicable to UA from different manufacturers and for diverse applications. Let one of the aircraft be the reference aircraft (Aircraft A) while the second aircraft is a colliding aircraft (Aircraft B). We assume that Aircraft A is moving along a straight path to point C with a constant velocity of $\overrightarrow{\mathbf{v}}_{\mathrm{A}}$. Similarly, Aircraft B travelling with a constant velocity $\overrightarrow{\mathbf{v}}_{\mathrm{B}}$ collide with Aircraft A at point D along the trajectory of Aircraft A.

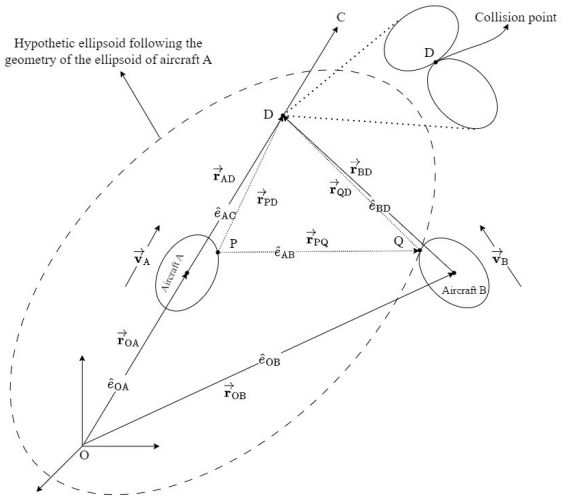


Fig. 2. Vector representation of the interaction of 2 aircraft.

The method deployed in this paper was to integrate the closest point of collision of the colliding aircraft to the geometry of the reference aircraft following the recommendations of [6]. This was achieved by encasing both aircraft in a hypothetical oblate-spheroid following the geometry of the reference aircraft as shown in fig. 2. We note that the axis of the oblate-spheroid comprises the aircraft geometry and a safety margin responsible to accommodate pilot/aircraft response, procedure safety margin, etc. [4]. The accuracy of the margin depends on the CNS equipment of the aircraft and air data and is statically configured. The time specifications for the safety margins are available in [4], [14].

Let Aircraft A be termed the reference aircraft while Aircraft B is the colliding aircraft. We assume that $P$ and $Q$ represent the closest point on the surface of the reference and colliding aircraft with Cartesian representation in (2) and (3) respectively.

$$P = C + x_0\hat{e}_0 + x_1\hat{e}_1 + x_2\hat{e}_2, \tag{2}$$

$$Q = C + y_0\hat{e}_0 + y_1\hat{e}_1 + y_2\hat{e}_2, \tag{3}$$

where $\hat{e}_i$ is a unit vector in the direction of the $i$th axis of the the ellipsoid. We note that the centre of the ellipsoid is relative to an earth-fixed reference frame as shown in fig. 2. Let the spherical representation of point $P$ be located at $(\rho, \theta, \phi)$ where $\rho$ is the distance from the origin of the ellipsoid and $\theta$ and $\phi$ are the polar and azimuth angles respectively. If we parameterise point $P$ to polar coordinates, then the distance between point $P$ and $Q$ is given with spherical coordinates as the Frobenius norm representation in (4).

$$F(\theta, \phi) = |Q - P(\theta, \phi)|^2. \tag{4}$$

The global minimum of (4) represents the closest distance between the reference and colliding ellipsoids. This minimum implies that the partial derivative of (4) equals zero.

$$\frac{\partial F}{\partial \theta} = 2(Q - P(\theta,\phi))\frac{\partial P}{\partial \theta} = 0, \tag{5a}$$

$$\frac{\partial F}{\partial \phi} = 2(Q - P(\theta,\phi))\frac{\partial P}{\partial \phi} = 0. \tag{5b}$$

We note that $\frac{\partial P}{\partial \theta}$ and $\frac{\partial P}{\partial \phi}$ are the tangents at point $P$ on the $\theta$ and $\phi$ polar axis respectively. However, to satisfy the conditions given in (5), the displacement vector, $(Q-P(\theta,\phi))$, from $Q$ to $P$ must be normal to the tangents of $\frac{\partial P}{\partial \theta}$ and $\frac{\partial P}{\partial \phi}$. This means that the displacement vector between $Q$ and $P$ is normal at least to one point on the reference ellipsoid if both aircraft are to collide. The point referred to as the collision point was depicted as $D$ in fig. 2. Without loss of generality, let $G$ given in (6) represent the ellipsoid equation from (1) characterising the dimensions of aircraft A. The equation for the normal at point $P$ was calculated as (7) where $\nabla G$ defines the gradient of $G$.

$$G = 1 - \Big(\frac{x_0}{a_0}\Big)^2 - \Big(\frac{x_1}{a_1}\Big)^2 - \Big(\frac{x_2}{a_2}\Big)^2. \tag{6}$$

$$\frac{\nabla G}{2} = \lambda\Big(\frac{x_0}{a_0^2}, \frac{x_1}{a_1^2}, \frac{x_2}{a_2^2}\Big). \tag{7}$$

We define the relations between the reference and colliding ellipsoids by equating the displacement vector between $Q$ and $P$ to the normal ellipsoid at point $P$. This implies that $\frac{\nabla G}{2} = Q - P$. Hence, we can find the relation between the point $P$ and $Q$ as given in (8), where $s$ is the displacement vector between both points.

$$y_0 = x_0\Big(1+\frac{\lambda}{a_0^2}\Big)\hat{e}_0; y_1 = x_1\Big(1+\frac{\lambda}{a_1^2}\Big)\hat{e}_1; y_2 = x_2\Big(1+\frac{\lambda}{a_2^2}\Big)\hat{e}_2, \tag{8}$$

where $\lambda$ is a scalar collision position parameter that defines the position of the nearest point of the colliding UA to the reference UA. For $\lambda > 0$, the colliding ellipsoid is not touching the reference ellipsoid, however, for $\lambda \leq 0$, a collision occurs between both UAs.

Let us assume that point $Q$ is $s$ distance from point $P$, (i.e. $|Q-P| = s$). The distance, $s$, can represent the vertical, lateral or longitudinal distance depending on the approach of the colliding aircraft. If we define the probability of having point $P$ at $(\rho,\theta,\phi)$ as $p(\rho,\theta,\phi)$, then the conditional probability of point $Q$ being $s$ distance from point $P$ can be represented as $p(s|\rho,\theta,\phi)$. We note that $s$ and $(\rho,\theta,\phi)$ are continuous random variables, hence we evaluate the probabilities over the possible regions of the variables. Let us define the probability of $Q$ located $s$ distance from $P$ as $p(s)$ given in (9).

$$p(s) = \int_0^{\pi}\int_0^{\infty} p(s|\rho,\theta,\phi)p(\rho,\theta,\phi)d\rho d\theta. \tag{9}$$

We note that $p(s) \equiv p(s \cap (\rho,\theta,\phi))$ represents the intersection of the occurrence of point $P$ and $Q$ at the described location. The integrals were used to extrapolate the collision point over the entire ellipsoidal geometry of the reference aircraft. For stability, we assume that both the reference and colliding aircraft do not rotate about any plane, therefore the influence of $\phi$, as the rotation angle from the initial meridian plane, on the probability function is irrelevant and precludes the use of the integral around the rotation axis.The solution to (9) to the fourth degree of the eccentricity, $\epsilon^4$, was presented in [18, 3.31 to 3.34] with an excerpt presented in (10).

$$p(s) = \begin{cases} p_{\mathrm{I}}(s), & 0 \leq s \leq 2b \\ p_{\mathrm{II}}(s), & 2b \leq s \leq 2a \\ 0, & \text{Otherwise} \end{cases} \tag{10}$$

$$p_{\mathrm{I}}(s) = \Big(\frac{3s^2}{a^3} - \frac{9s^3}{4a^4} + \frac{3s^5}{16a^6}\Big) + \epsilon^2\Big(\frac{3s^2}{2a^3} - \frac{3s^3}{2a^4} + \frac{3s^5}{16a^6}\Big) + \epsilon^4\Big(\frac{9s^2}{8a^3} - \frac{27s^3}{20a^4} + \frac{9s^5}{40a^6}\Big) + \mathcal{O}(\epsilon^6).$$

$$\begin{aligned} p_{\mathrm{II}}(s) = X\epsilon^2(1-X^2)\Bigg[&\frac{p_{\mathrm{I}}(s) - \mathcal{O}(\epsilon^6)}{\epsilon^2(1-X^2)} + \\ &\left(\frac{117s^2}{96a^3} - \frac{171s^3}{192a^4} - \frac{9s^4}{32a^5} + \frac{27s^5}{128a^6} - \frac{9s^2(s^2-a^2)^2}{32a^6}\ln\Big(\frac{s}{a}-1\Big)\right) \\ &+ \epsilon^2\left(\frac{1251s^2}{768a^3} - \frac{2619s^3}{2560a^4} - \frac{171s^4}{256a^5} + \frac{2259s^5}{15360a^6} + \frac{27s^7}{512a^8}\right) \\ &- \epsilon^2\ln\Big(\frac{s}{a}-1\Big)\left(\frac{171s^3(s^2-a^2)}{256a^6} - \frac{63s(s^2-a^2)}{256a^4}\right) \\ &+ \epsilon^2X^2\left(-\frac{261s^2}{256a^3} + \frac{711s^3}{2560a^4} + \frac{135s^4}{256a^5} + \frac{1323s^5}{5120a^6} - \frac{63s^7}{512a^8}\right) \\ &+ \epsilon^2X^2\ln\Big(\frac{s}{a}-1\Big)\left(\frac{135s^3(s^2-a^2)}{256a^6} - \frac{27s(s^2-a^2)}{256a^4}\right)\Bigg] \\ &+ \mathcal{O}(\epsilon^6), \end{aligned}$$

where $a$ and $b$ are the major and minor axis of the well-clear boundary between the colliding and reference aircraft, $\epsilon = \sqrt{1-\frac{b^2}{a^2}}$, $X = \frac{\sqrt{1-\epsilon^2}}{\epsilon}\sqrt{\frac{4a^2}{s^2}-1}$ and $\mathcal{O}(\epsilon^6)$ limits the function, $p(s)$, as it tends to $\epsilon^6$. The proof of (10) was presented in [18]. We note that $p(s)$ is a function of the distance, $s$, the axis of the hypothetical oblate-spheroid, $a$, and the eccentricity, $\epsilon$. For $s > 2a$, the reference and colliding aircraft are far from each other so they are not endangered from a collision.

### C. Collision velocity

Consider that the distance between the first collision point on Aircraft A and B to the collision point D at $t \in (t_0, t_1)$ is given in (11) and (12) respectively.

$$D = P + \overrightarrow{\mathbf{v}}_{\mathrm{A}} t\hat{e}_{\mathrm{AD}}, \tag{11}$$

$$D = Q + \overrightarrow{\mathbf{v}}_{\mathrm{B}} t\hat{e}_{\mathrm{BD}}, \tag{12}$$

where $\hat{e}_{\mathrm{iD}}$ represents the unit vector from points $i \in \{\mathrm{A}, \mathrm{B}\}$ to the collision point at D, $t_0$ and $t_1$ are the initial and final observation time respectively. Hence, we have that

$$\lambda\Big(\frac{x_0}{a_0^2}, \frac{x_1}{a_1^2}, \frac{x_2}{a_2^2}\Big) = \overrightarrow{\mathbf{v}}_{\mathrm{A}} t\hat{e}_{\mathrm{AD}} - \overrightarrow{\mathbf{v}}_{\mathrm{B}} t\hat{e}_{\mathrm{BD}}. \tag{13}$$

Following from the assertion of [19, eq. 2], the instantaneous change of $s$ with respect to time, $t$ is given as (14).

$$\frac{\partial s}{\partial t} = \overrightarrow{\mathbf{v}}_{\mathrm{A}} \hat{e}_{\mathrm{AD}} - \overrightarrow{\mathbf{v}}_{\mathrm{B}} \hat{e}_{\mathrm{BD}} \equiv v. \tag{14}$$

As aircraft A and B approach collision point D, the distance $|Q - P|$ tends to zero, therefore, $\lambda = 0$ and $v \geq 0$ just before the instantaneous collision time assuming that the aircraft is not manoeuvred. This implies position and velocity share the same probability space.

### D. Collision and conflict probability

For collision between aircraft A and B to occur, the distance between both aircraft, $s$, should be less than or equal to the distance-based separation minima, $\bar{S}$. We note that $\bar{S}$ was configured to include a safety margin which provides for pilot/aircraft response, CNS equipment performance and air data, etc. [4]. Therefore, the collision probability, $p(\bar{S} \geq s)$, is defined as the probability that aircraft A will collide with aircraft B at the time, $t$, given that aircraft locations were measured with respect to time. The collision probability defines the collision risk model (CRM) and is also referred to as instantaneous probability of collision (IPC) [20]. Analytically, $p(\bar{S} \geq s)$ is the tail distribution of $p(\bar{S} \leq s)$ and can be obtained by the equations given in (15) and (16).

$$p(\bar{S} \geq s) = 1 - p(\bar{S} \leq s) = p(s \leq \bar{S}). \tag{15}$$

$$p(\bar{S} \geq s) = 1 - \int_0^{\bar{S}} p(s)ds. \tag{16}$$

*(a) Theoretically, the integral bound begins from $-\infty$ to $\bar{S}$, however, the feasible range from 0 to $\bar{S}$ is considered since we exclude negative separation distance between both aircraft due to* (10).

*(b) For $0 \leq \bar{S} \leq 2b$, $\int_0^{\bar{S}} p(s)ds = \int_0^{\bar{S}} p_{\mathrm{I}}(s)ds$ while for $2b \leq \bar{S} \leq 2a$, $\int_0^{\bar{S}} p(s)ds = \int_0^{2b} p_{\mathrm{I}}(s)ds + \int_{2b}^{\bar{S}} p_{\mathrm{II}}(s)ds$*

*(c) Due to the complexity of $p_{II}(s)$, the solution to* (16) *is obtained using numerical integration.*

It is essential to note that the separation minima discussed in this paper are the closest safe distance that a colliding aircraft can approach from the boundary of the reference aircraft before the probability of collision exceeds the recommendation. It contrasts the separation minimum discussed in [4] which is the distance between the 2 proximate aircraft.

Furthermore, if $p(v_A)$ and $p(v_B)$ represent the independent probabilities of aircraft A and B travelling with a velocity of $v_A$ and $v_B$ respectively. Following [16], we can formulate the conflict probability, $p_{s,v}(s, v)$, as the joint probability of aircraft A and B separated by $\bar{S} \geq s$ and travelling with a velocity of $p(v_A)$ and $p(v_B)$ respectively as (17).

$$p_{s,v}(s, v) = p(\bar{S} \geq s)p(v), \tag{17}$$

where $p(v) = p(\overrightarrow{\mathbf{v}}_{\mathrm{A}} \hat{e}_{\mathrm{AD}} - \overrightarrow{\mathbf{v}}_{\mathrm{B}} \hat{e}_{\mathrm{BD}})$. We note that the probability of an aircraft travelling with a velocity of $v_{\mathrm{A}}$ or $v_{\mathrm{B}}$ to any particular direction is normally distributed, then $p(v)$ will also be normally distributed with mean $\mu = \mu_{\mathrm{A}} - \mu_{\mathrm{B}}$ and variance $\sigma = \sigma_{\mathrm{A}} + \sigma_{\mathrm{B}}$. This assertion is commonly used in literature and can be obtained from the application of the central limit theorem (CTL) which shows that with the evaluation of a significant sample of aircraft, the probability of their velocity follows a normal distribution. Understanding the conflict probability model allows for the characterisation of collision risk modelling analysis.

### E. Dynamic separation minima

The separation minima link to the collision probability model via the parameter, $\bar{S}$. In conventional aviation with manned operation, $\bar{S}$ is statically configured as the separation minima with values given in [11]. From the oblate-spheroid geometry, if the distance between the reference and colliding aircraft is greater than $2a$, then both aircraft have no interaction implying no collision or that the collision probability is zero. Therefore, we can establish that the range of separation minima is $0 \leq \bar{S} \leq 2a$ with equality describing the bounds of $\bar{S}$. Lowering the value of $\bar{S}$ cause fewer options for manoeuvrability, therefore, we revise the range by equating the collision probability to the boundaries of $p(\mathrm{MAC}|\mathrm{NMAC})$ and $p(\mathrm{NMAC}|\mathrm{WCV})$. WCV is the Well-clear violation which represents when the failure of the mitigation to prevent the bridge of the well-clear boundary. The separation minima characterises the dynamic separation model, $\bar{S}$, which can be obtained using the following procedure:

(a) Input the length of the major axis of the oblate-spheroid, the eccentricity and the collision probability.
(b) Numerically solve the boundary equation $\min(p(\bar{S} \leq s)) - p(\bar{S} \geq s) = 0)$ for $\bar{S}$.
(c) Output the value of $\bar{S}$.

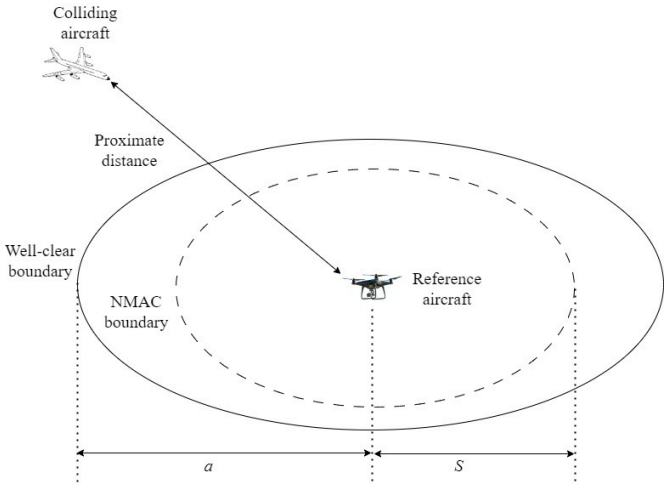


Fig. 3. 2D figurative characterisation of separation minima.

The separation minima boundary for an interaction between sUAS and a manned aircraft was presented in fig. 3. Although

this form of interaction is expected to be few in practice due to the different operating altitudes, fig. 3 is a representation of the interaction of any 2 proximate aircraft.

## IV. Numerical Assessment

In this section, we evaluate the analytical representations presented in the paper. In figs. 6 and 5, we have compared the collision probability with a Monte Carlo simulation for different values of eccentricity, $\epsilon$. For the Monte Carlo simulation, we generated $10^5$ normal distributed random points with zero mean and $0.5$ standard deviation in an oblate-spheroid with its major axis, $a = 1$, hence the largest possible distance between any two points is 2 Km. We evaluated the probability of having the randomly generated points at a specified distance within the region of $[0, 2a)$.

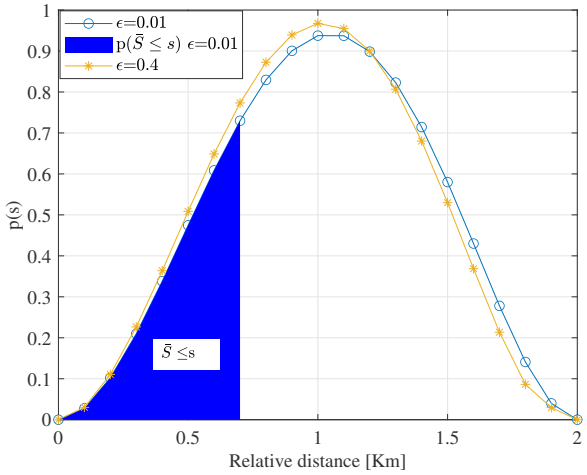


Fig. 4. A plot of the probability distribution given in (10) with varying relative distance between any 2 aircraft for $a = 1$.

Figure 4 shows a graphical representation of the probability density function (PDF) that the distance between two aircraft in an oblate-spheroid is less than twice the major axis. Using different eccentricity values, we observe a shift in the distribution but with the same mean and variance showing that the ratio of the major and minor axis of the spheroid has little significant impact on the distribution. The shaded part of fig. 4 depicts the area under consideration when computing the collision probability from a hypothetical separation distance.

The probability distribution of the distance between the reference and colliding aircraft was presented in fig. 5. Compared with the Monte Carlo simulation, we observe that both functions are similar for different values of eccentricity with slight deviation when $s > a$. A similar observation was obtained from the conflict probability plot in fig. 6 in terms of the comparison to the Monte Carlo simulations and the effect of eccentricity. The observation shows that designing the major axis as a parameter of the separation minima can allow for its variation. Figure 6 showed that as the distance between 2 aircraft increases, the collision probability reduces from certain collision when the distance is 0 to the little or no

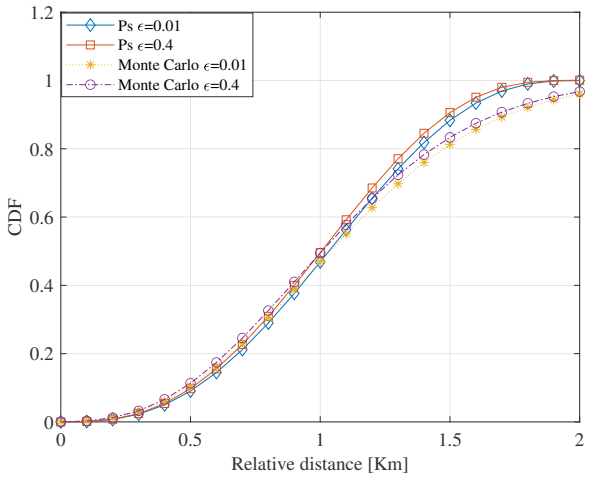


Fig. 5. Comparing the cumulative distribution of $p(s)$ to the probability obtained from Monte Carlo simulation.

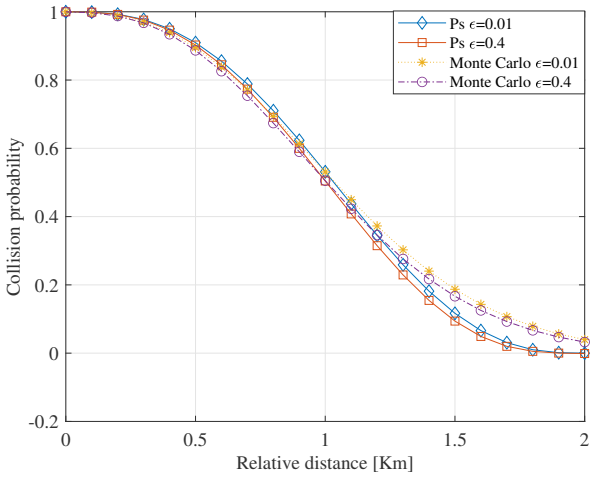


Fig. 6. Evaluating collision probabilities again the relative distance between 2 aircraft.

collision as the distance between both aircraft approach twice the longest dimension, $2a$.

TABLE I
Dynamic separation minima for $a = 500$ft

| $p(S \geq s)$ | Eccentricity | $S$ (ft) |
|---|---|---|
| 0.01 | 0.4 | 109.5119 |
| 0.01 | 0.01 | 112.6836 |
| 0.2 | 0.4 | 332.3500 |
| 0.2 | 0.01 | 341.9321 |

TABLE II
DYNAMIC SEPARATION MINIMA FOR $a = 250$FT

| $p(S \geq s)$ | Eccentricity | $S$ (ft) |
|---|---|---|
| 0.01 | 0.4 | 54.7560 |
| 0.01 | 0.01 | 56.3418 |
| 0.2 | 0.4 | 166.1750 |
| 0.2 | 0.01 | 170.9660 |

Furthermore, Tables I and II provide the computed separation minima for when the length of the major axis is 500ft and 250ft respectively. The major axis length herein is obtained from the oblate-spheroid modelling after the boundary of the aircraft. Higher values of eccentricity lead to a decrease in the length of the minor axis which invariably compress the geometry of the spheroid. Hence with high eccentricity, the smaller the geometry which causes Tables I and II to show lower separation minima. When the collision probability increases, the separation minima also increases to provide an extra safety gap. These observations show the dependence of separation minima on the dimensions of the geometry formed by the proximate aircraft and thus, the need for separation dynamism.

## V. CONCLUSION

We have presented a model for developing dynamic separation minima from the collision model based on the variation of the geometry around the aircraft. We related the aircraft geometry to its dimension and the inherent separation required to manoeuvre the aircraft. Using an oblate spheroid as the base geometry of an aircraft, we modelled the collision probability. We determined the parameters of the geometry and by setting the major axis of the aircraft geometry we showed that for various configurations of the geometry, the separation minima can be dynamically configured.

## ACKNOWLEDGMENT

This work was funded by Innovate UK under grant agreement numbers 10025964 and 10024815, as part of the Future Flight Challenge (Phase 3) program: projects Blueprint and High-intensity Autonomous Drone Operations (HADO) respectively.

## REFERENCES

[1] "Unmanned aircraft system operations in UK airspace – policy and guidance CAP 722," 2022, Civil Aviation Authority (CAA), Ninth Edition Amendment 1.

[2] G. Bakker and H. Blom, "Air traffic collision risk modelling," in *Proceedings of 32nd IEEE Conference on Decision and Control*, 1993, pp. 1464–1469 vol.2.

[3] S. Bijjahalli, A. Gardi, N. Pongsakornsathien, and R. Sabatini, "A unified collision risk model for unmanned aircraft systems," in *2021 IEEE/AIAA 40th Digital Avionics Systems Conference (DASC)*, 2021, pp. 1–10.

[4] "CARE-ASAS Activity 3: Investigation of experience in modelling and determining separation minima," 2002, CARE-ASAS Action Activity 3, version 2.1.

[5] S. Förster, M. Schultz, and H. Fricke, "Probabilistic prediction of separation buffer to compensate for the closing effect on final approach," *Aerospace*, vol. 8, no. 2, 2021. [Online]. Available: https://www.mdpi.com/2226-4310/8/2/29

[6] "ICAO Cir 319, A unified framework for collision risk modelling in support of the manual on airspace planning methodology for the determination of separation minima (Doc 9689)," 2009, International Civil Aviation Organization.

[7] K. Blin, M. Akian, F. Bonnans, E. Hoffman, C. Martini, and K. Zeghal, "A stochastic conflict detection model revisited," *American Institute of Aeronautics and Astronautics*, August 2000.

[8] R. Xiong, Y. Wang, P. Tang, N. J. Cooke, S. V. Ligda, C. S. Lieber, and Y. Liu, "Predicting separation errors of air traffic controllers through integrated sequence analysis of multimodal behaviour indicators," *Advanced Engineering Informatics*, vol. 55, p. 101894, 2023. [Online]. Available: https://www.sciencedirect.com/science/article/pii/S1474034623000228

[9] Q. Cai, H. Jie, Aang, and A. Sameer, "Collision risk assessment of reduced aircraft separation minima in procedural airspace using advanced communication and navigation," *Chinese Journal of Aeronautics*, 2022.

[10] J. Delgado-Aguilera, V. Gómez, Comendador, M. Zamarreño, Suárez, F. Pérez, Moreno, C. Verdonk, Gallego, and R. Arnaldo Valdes, "Safety performance functions to predict separation minima infringements in en-route airspace," *Aircraft Engineering and Aerospace Technology*, vol. 94, no. 9, 2022.

[11] "Application of separation minima north atlantic region," December 2022, ICAO European and North Atlantic Office NAT ASM-1st Edition, Amendment 11.

[12] "UAS ATM CARS common altitude reference system: Discussion document," 2018, European Organisation for the Safety of the Air Navigation (EUROCONTROL), Directorate of European Civil-Military Aviation (DECMA), Aviation Cooperation and Strategies Division (ACS).

[13] A. Weinert, S. Campbell, A. Vela, D. Schuldt, and J. Kurucar, "Well-clear recommendation for small unmanned aircraft systems based on unmitigated collision risk," *Journal of Air Transportation*, vol. 26, no. 3, pp. 113–122, 2018. [Online]. Available: https://doi.org/10.2514/1.D0091

[14] "Standard specification for detect and avoid system performance requirements," 2020, ASTM International F3442/F3442M-20.

[15] T. Rad, S. Schönhals, and P. Hecker, "Dynamic separation minima coupled with wake vortex predictions in dependent runway configurations," *Proceedings of the Institution of Mechanical Engineers, Part G: Journal of Aerospace Engineering*, vol. 228, no. 8, pp. 1450–1457, 2014. [Online]. Available: https://doi.org/10.1177/0954410013496517

[16] J. F. Shortle, Y. Xie, C. H. Chen, and G. L. Donohue, "Simulating collision probabilities of landing airplanes at nontowered airports," *SIMULATION*, vol. 80, no. 1, pp. 21–31, 2004. [Online]. Available: https://doi.org/10.1177/0037549704042028

[17] R. A. Paielli and H. Erzberger, "Conflict probability estimation for free flight," in *AIAA Meeting Papers on Disc*, 1997.

[18] M. Parry and E. Fischbach, "Probability distribution of distance in a uniform ellipsoid: Theory and applications to physics," *Journal of Mathematical Physics*, vol. 41, no. 4, 2000.

[19] H. Blom and G. Bakker, "Conflict probability and incrossing probability in air traffic management," in *Proceedings of the 41st IEEE Conference on Decision and Control, 2002.*, vol. 3, 2002, pp. 2421–2426 vol.3.

[20] G. Ulises, E. Núñez and L. E. Glenn, "Relating collision probability and separation indicators in spacecraft formation collision risk analysis," *Journal of Guidance, Control, and Dynamics*, vol. 45, no. 3, 2022.

2023-11-10

# Dynamic separation minima prediction with collision risk modelling (CRM)

Nnamani, Christantus O.

IEEE

Nnamani CO, Gong T, Xu Y, Tsourdos A. (2023) Dynamic separation minima prediction with collision risk modelling (CRM). In: IEEE/AIAA 42nd Digital Avionics Systems Conference (DASC) 2023, 1-5 October 2023, Barcelona, Spain

https://doi.org/10.1109/DASC58513.2023.10311317